K. Kussmaul and R. Stegmeyer**

The Thermal Fatigue Behaviour of a Thick-Walled, Notched Hollow Cylinder

REFERENCE Kussmaul, K. and Stegmeyer, R., **The thermal fatigue behaviour of a thick-walled, notched hollow cylinder**, *Biaxial and Multiaxial Fatigue*, EGF 3 (Edited by M. W. Brown and K. J. Miller), 1989, Mechanical Engineering Publications, London, pp. 301–315.

ABSTRACT The fatigue behaviour of a material is generally investigated with small test bars which are mechanically deformed at constant temperature. There is no guarantee, however, that the results obtained exactly reflect the actual behaviour of thermally loaded components, especially large shafts. In order to find out whether the results from laboratory tests can be applied to real components, some specimens which simulate a turbine shaft geometry were exposed to temperature cycles. In this context, the crack initiation behaviour was of special importance. The best correlation between crack initiation curves obtained from isothermal and single-axial loading tests was established by means of the equivalent von Mises strain. When analysing a component, life prediction is based on computed strains via the finite element method. The accuracy of the numerical results was judged by comparison with those results obtained by measurement.

Introduction

During the non-steady state operation of components subject to thermal loads created during start-up and run-down procedures, temperature-induced strains of an essentially multiaxial nature occur as the result of non-constant temperatures. In comparison with these strains, the influence of mechanical loads from, for example, internal pressure or centrifugal force, are secondary. The service life of components of this kind is, therefore, essentially determined by thermally induced strains.

Previous investigations of the low cycle fatigue characteristics of components of this kind were carried out on small round specimens subjected to single-axial loads. In the experiments described below, however, the actual component was simulated, i.e., a specimen similar to the component was subjected to temperature cycles. The turbine shaft was selected as representative of all the components affected. The axisymmetric geometry and the straightforward nature of the load involved can be simulated in experiments with relative simplicity. Accordingly, the experimental specimen was a thick-walled hollow cylinder ($d_o/d_i = 1.67$). Circumferential grooves were used, firstly to simulate the shoulder of the turbine shaft, and secondly to provide a general increase in local strains. The ratio of length to diameter was optimized by means of a numerical stress analysis via the finite element method. The final shape of the specimen

* Staatliche Materialprüfungsanstalt (MPA), Universität Stuttgart, Pfaffenwaldring 32, 7000 Stuttgart 80, FRG.

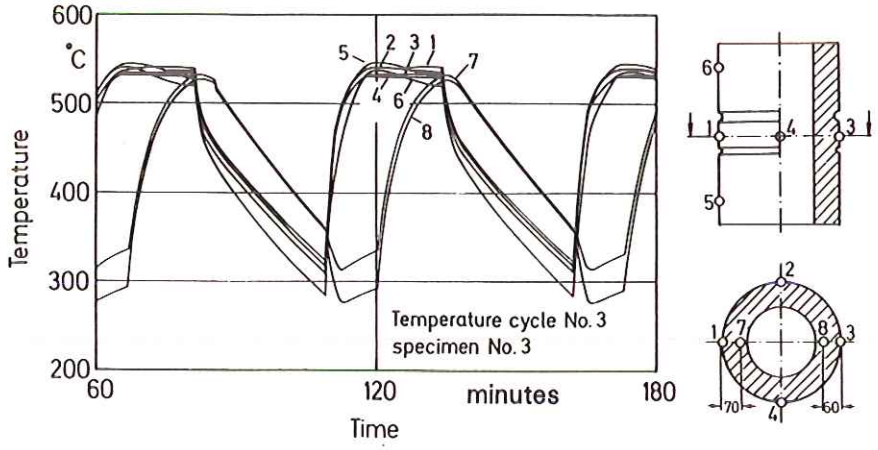

Fig 1 Specimen geometry, thermocouple location, and cyclic temperature profiles

(540 mm length, 360 mm outside diameter) is indicated in Fig. 1, with details given in a companion paper (**1**). The experimental material was the heat-resistant turbine shaft steel 28 CrMoNiV 4 9, Table 1. This steel offered the advantage that a large quantity of experimental data, previously determined isothermally in conventional tests, was available for comparison purposes.

Notation

a	Crack depth
c	Thermal capacity
d_o	Outer diameter
d_i	Inner diameter
E	Modulus of elasticity
K	Stress intensity factor
N	Number of cycles
N_A	Number of cycles to crack initiation
R	Notch root radius
t	Time
T	Temperature
α	Coefficient of thermal expansion
ε	Strain
ε_r	Radial strain
ε_t	Tangential strain
ε_z	Axial strain
ε_v	Equivalent strain
μ	Poisson's ratio
ϱ	Density
σ	Stress

Table 1 Chemical composition of the material 28 CrMoNiV 4 9 and its heat treatment

C	*Si*	*Mn*	*P*	*S*	*Cr*	*Ni*
0.26	0.17	0.45	0.016	0.012	1.1	0.58
Mo	*V*	*Al*	*Sn*	*Sb*	*Cu*	*As*
0.9	0.27	0.005	0.026	0.003	0.09	0.031

Heat treatment: 950°C in oil 5 hours + 720°C in air 8 hours; cooling velocity 20°C per hour after each heat treatment.

Experimental assembly

Figure 1 shows one of five different temperature cycles which are similar in form, but with a different temperature drop to give a different strain range (Table 2) to which the specimens were subjected. In order to be able to achieve these cycles, it was necessary to develop and construct a special test facility matched to the shape of the specimen. This facility is described in reference (1). Temperature was measured with Ni–Cr/Ni thermocouples, not only at the surface, but also inside the wall. It was also necessary to record the strains generated at the surface of the specimen, and for this purpose a special clip gauge was developed that was matched to the requirements of this problem.

Experimental results

Crack development and crack propagation

With cyclic deformation, incipient cracks generally occur at the surface. On the current large-scale specimen the cracks, located by a Magnaflux inspection,

Table 2 Test parameters

Specimen No.	*Notch radius (mm)*	*Maximum temperature (°C)*	*Minimum temperature (°C)*	*Strain range, $\Delta\varepsilon_z$ at the base of the notch (%)*
1	5.0	530	195	1.48
2	5.0	530	195	1.48
3	5.0	530	275	0.88
	20.0			0.53
4	5.0	530	335	0.50
	20.0			0.37
5	5.0	530	380	0.45
	20.0			0.30
6	10.0	530	380	0.35
	15.0			0.32
7	22.5	530	380	0.28
	25.0			0.26
8	5.0	530	380	0.45
	10.0			0.35

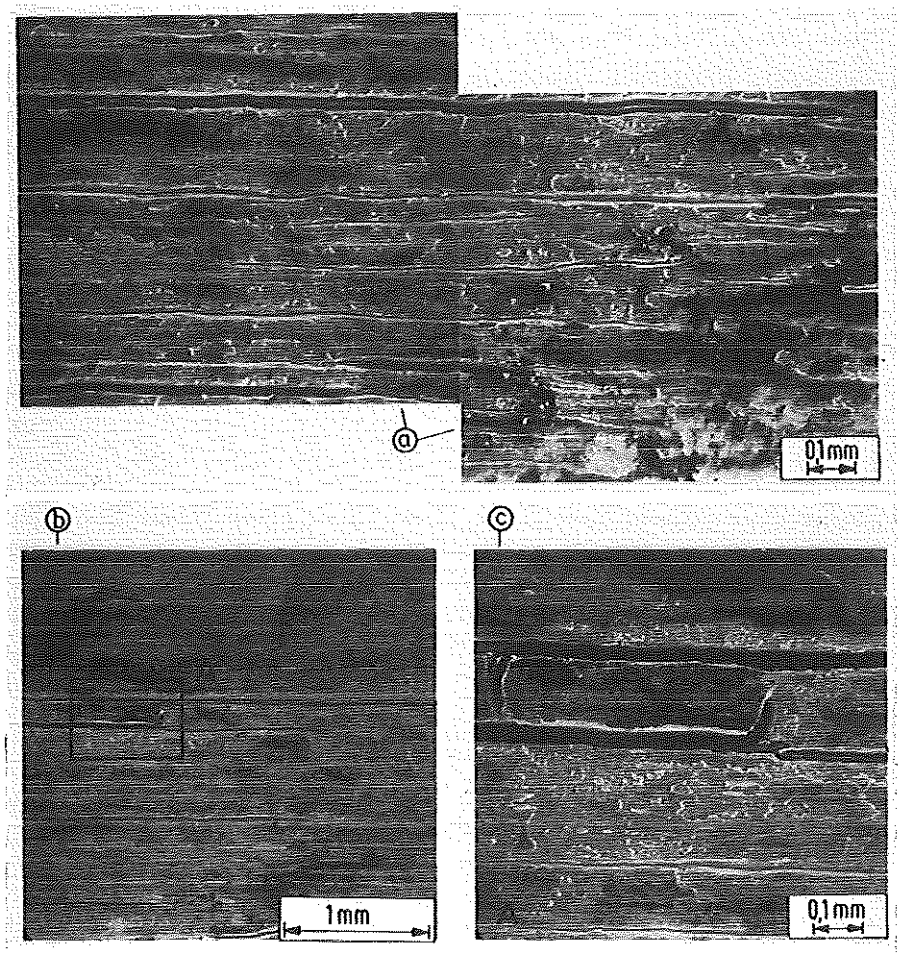

Fig 2 Circumferentially-oriented surface cracks at the base of a notch: (a) specimen no. 4; (b) specimen no. 4 (other location); (c) enlargement of (b)

were evaluated as incipient cracks. After the end of the experiment, the cracks were subjected to a metallographic examination and the exposed crack surfaces to a fractographic examination. In the crack development phase, a number of small circumference-oriented surface cracks form in the base of the notch with a parallel offset (Fig. 2). As the experiment continues, the cracks join up and produce one or more continuous circumferential cracks. This joining of individual cracks need not take place on a single plane, but can meet in the axial direction through tearing (Fig. 2). The formation of cracks at the base of the notch depends on the strain amplitude. Large alternating plastic deformations (large plastic zone) produce a broad crack field. As the strain amplitude is reduced, for the same notch radius, the width of the crack field and thus the

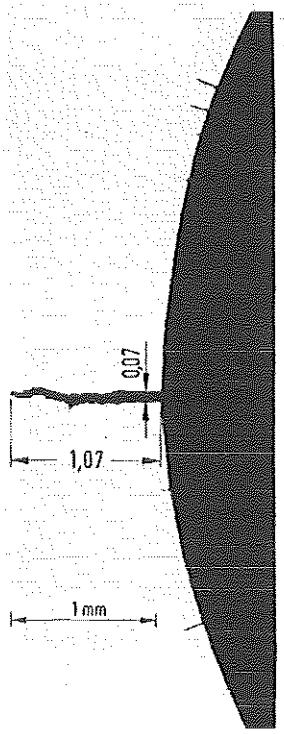

Fig 3 Main crack at the centre of the base of a 5 mm radial notch

number of parallel cracks is reduced. In almost all cases, a main central crack (Fig. 3) develops at the centre of the base of the notch as the experiment is continued. With increasing duration, a heavy oxide layer forms. The oxygen in the surrounding air is transported to the crack tip and affects the crack propagation. The exposed crack surfaces were carefully freed of the layer of scale. Figure 4(a) shows the opened up fracture surface of a sample and Fig. 4(b) the striations at point A. The number of fractographically-recorded striations correspond to the number of temperature cycles following the crack development.

Taking the crack growth equation in accordance with Paris (2)

$$\frac{da}{dN} = C \cdot \Delta K^n \tag{1}$$

da/dN can be determined in this case from the width of the amplitude striation. The stress intensity, K, was calculated by means of approximation equations; details see reference (3). With tests of different stress intensity ranges, ΔK (different temperature cycles), which produce different width of the striations, the constants C and n in the Paris law could be determined.

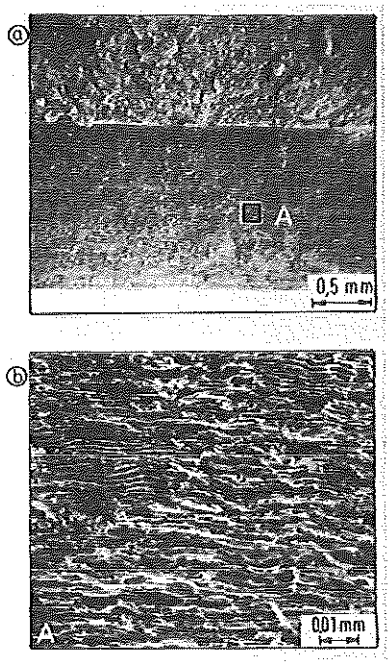

Fig 4 Fatigue striations on crack fracture surface: (a) specimen no. 4; (b) enlargement of (a)

Incipient crack characteristics

Using cyclic thermal strains it was possible to produce cracks in the base of the notch in a total of eight specimens, each with two circumferential notches and, in certain cases, different notch radii, Table 2. The experimental results are shown in Fig. 5(a) as an incipient crack, i.e., the measured axial strain at the base of the notch is shown as a function of the number of temperature cycles up to the point of crack development. A comparison of these results with the results from isothermal experiments on round specimens (**4**) subjected to axial load at 530°C reveals notable differences. In this case, the curve without hold time is used as a reference, since no creep strains were detected on the large-scale specimen. Both methods of test include the influence of oxidation on crack initiation and growth. The large differences are due to the different incipient crack detection methods used. With the large-scale specimen experiments, it was possible to identify the incipient crack positively after a crack depth of approximately 0.1 mm, while, with the single-axial, strain controlled, standard laboratory specimens, where incipient cracking is prognosticated by the beginning of load decrease, only cracks of approximately 1 mm depth can be clearly observed. Being able to compare the number of cycles to crack initiation, which were ascertained by different means, the incipient crack depth

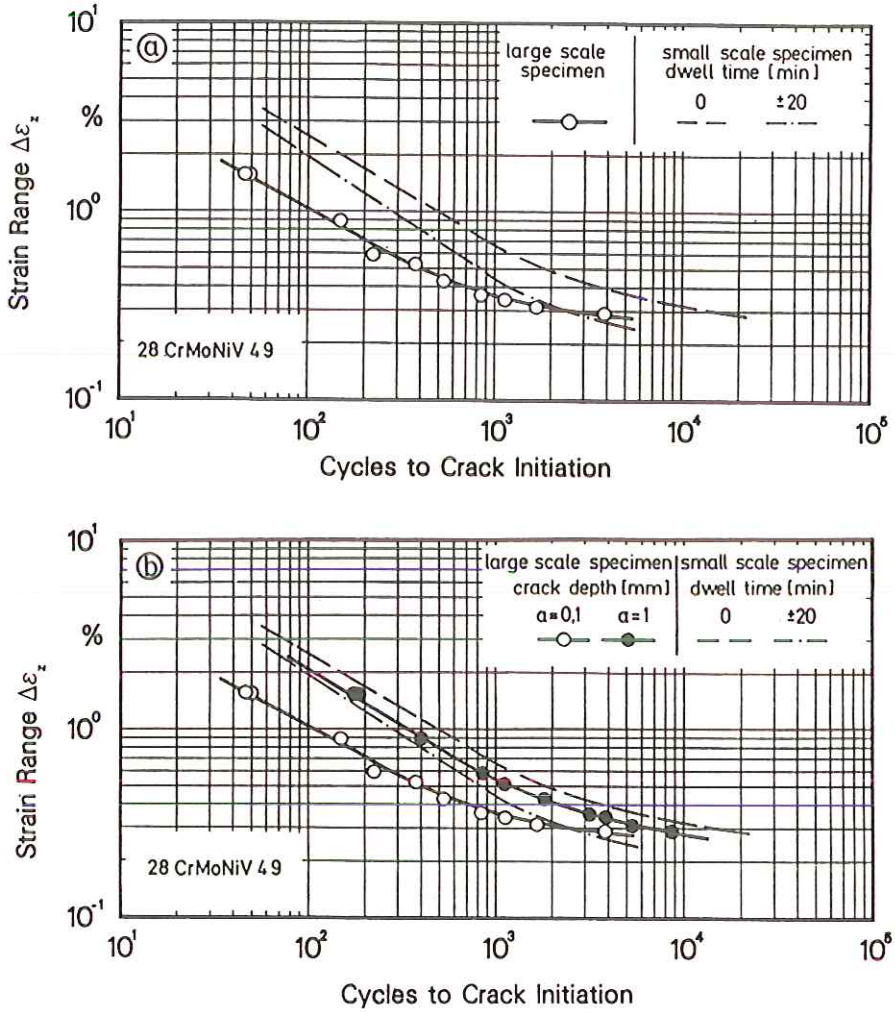

Fig 5 Crack initiation curves: (a) large scale specimens; (b) comparison with 0.1 mm and 1 mm crack depths

of 0.1 mm in the large scale specimen was extrapolated by means of the Paris law up to a crack depth of 1 mm. The resulting number of cycles (0.1 mm + 0.9 mm crack growth) for different large scale specimens in relation to the laboratory specimens is shown in Fig. 5(b). The parameter used for comparison is the axial strain amplitude.

Theoretical determination of stress

The strain characteristics of components subjected to thermal load on a number of axes can be investigated both by empirical methods, e.g. Neuber, and by

numerical methods, e.g., finite elements. When used appropriately, the finite element method (FEM) produces the highest accuracy with complex structures. In the following, particular reference is made to FEM application to the large-scale specimens, and an assessment is made of the calculated strains by comparing these with measured strains.

Application of the numerical finite element method to large-scale specimens

The calculations for the large models were carried out in two separate stages. In the first calculation, the transient temperature field was calculated for various points in time, using the temperature measured at the surface of the specimens in each case (**5**). The temperature calculated for each idealized node was then multiplied by the associated coefficient of thermal expansion and incorporated into the elastoplastic calculation (**6**) as the initial strain. It was assumed that the model was free of internal stress at the beginning of the calculation. Both calculations were based on the same number and type of elements; there were, however, internal differences in the elements resulting from the choice of statement functions (temperature or displacement statement). Due to the axisymmetry of the models, axisymmetric ring elements were used. In order to achieve the most accurate results possible, the following material properties were specified as a function of temperature:

Thermal conductivity $\lambda = \mathrm{f}(T)$
Thermal capacity $c = \mathrm{f}(T)$
Coefficient of thermal expansion $\alpha = \mathrm{f}(T)$
Density $\varrho = \mathrm{f}(T)$
Modulus of elasticity $E = \mathrm{f}(T)$
Stress/strain relationship $\sigma = \mathrm{f}(\varepsilon, T)$

The mathematical relationship between the individual material properties and temperature was described with higher-order polynomials. In contrast to calculations with a monotonic load, in which the hardening of the material is described by the static yield curve, the calculation was carried out with the cyclic yield curve at $N/N_A = 0.5$. The cyclic yield curves for particular temperatures were approximated by a logarithmic statement incorporating temperature as the third variable. The procedure is outlined below

$$\sigma_{T_1} = A_{T_1} + B_{T_1} \cdot \ln \varepsilon + C_{T_1} \cdot \ln^2 \varepsilon + D_{T_1} \cdot \ln^3 \varepsilon$$
$$\sigma_{T_n} = A_{T_n} + B_{T_n} \cdot \ln \varepsilon + C_{T_n} \cdot \ln^2 \varepsilon + D_{T_n} \cdot \ln^3 \varepsilon \qquad (2)$$

where the constants for a given temperature are

$$A_T = a_A + b_A \cdot \sin T + c_A \cdot \sin^2 T$$

through

$$D_T = a_D + b_D \cdot \sin T + c_D \cdot \sin^2 T$$

while stresses at the given temperature are

$$\sigma_T = A_T + B_T \cdot \ln \varepsilon + C_T \cdot \ln^2 \varepsilon + D_T \cdot \ln^3 \varepsilon$$

The equivalent stress or strain was calculated using the von Mises method.

Representation of the numerical results and comparison with the measured values

Numerical analysis was carried out for five of the total of eight specimens studied, making allowance for the different notch radii. Extensive temperature measurements were carried out only at the start of the series of experiments. Due to the fact that temperature curves measured for the interior and exterior surfaces of the model are specified as parameters for the calculation, a calculation/measurement comparison is meaningful only for the points inside the wall. Figure 6 shows this comparison for various points in time within a cycle. The slight differences (max. 10°C) are due, in part to the slight temperature differences detected in the experiment around the circumference of the

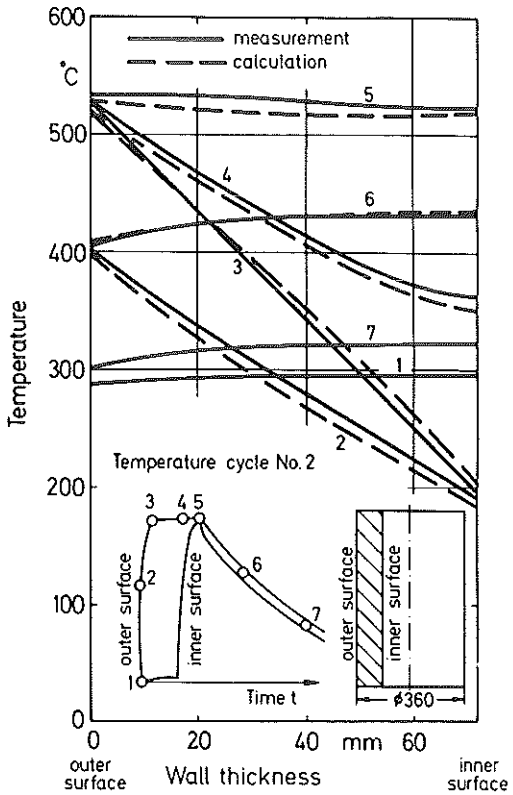

Fig 6 Comparison of the measured and calculated temperature curves in the wall at various points in time within a cycle

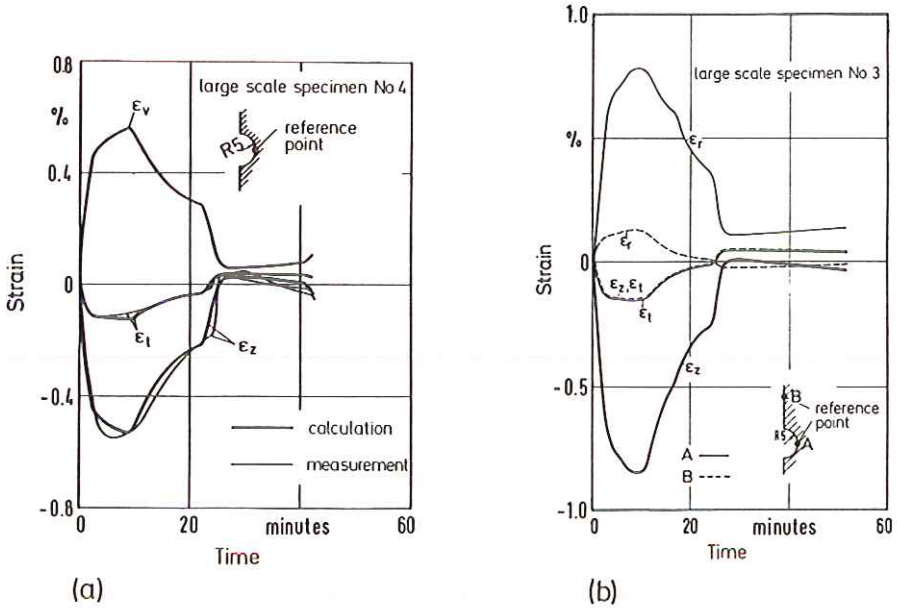

Fig 7 Strain as a function of time: (a) Comparison of the measured and calculated strains at the base of the notch; (b) comparison of the strain components at the undisturbed outer surface and at the base of the notch

specimen, and partly to the temperature decrease along the length of the specimen in the direction of the front face; no allowance is made for these effects in the calculation. Figure 7(a) shows a comparison between calculated strains and experimental results. Since the calculations are based on cyclic yield curves at half the number of cycles required for an incipient crack ($N/N_A = 0.5$), the strains measured for $N/N_A = 0.5$ were also used for the comparison. The correlation can be considered to be adequate.

Figure 7(b) shows a comparison of the strain components at the undisturbed outer surface and those at the base of the notch. As was to be expected with a pure temperature load, the axial and circumferential strains at the smooth surface are of identical value. The notch did not act as a centre of disturbance to affect the circumferential strains at the base of the notch.

Figure 8(a) shows an evaluation of the equivalent strain at time $t = 2.5$ minutes in the form of contour lines. In line with the original aim in the selection of the model, the peripheral influence of the specimen in the vicinity of the notches has died away. On the other hand, the notch influences the strain curves in the notch cross-section almost up to the centre of the wall thickness.

Figure 8(b) shows the development of the plastic zone as the surface temperature rises. In addition to plastic deformation at the base of the notch, the inner surface also suffers slight plasticity.

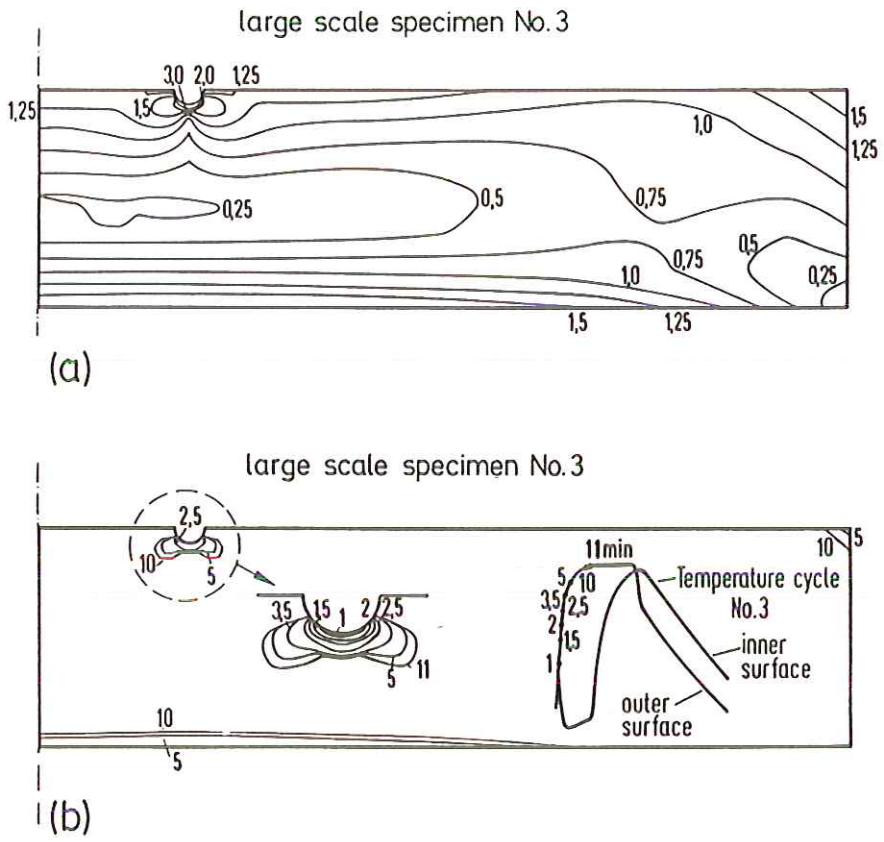

Fig 8 (a) Contour lines of equivalent strain ($\times 10^{-3}$) 2.5 minutes after the start of a cycle; (b) development of the plastic zone with time in minutes as the surface temperature rises

The mathematically-determined strain amplitude depends strongly on the selected hardening rule; isotropic or kinematic. Figure 9(a) shows the influence of hardening rule, taking the associated strains as examples.

In contrast to calculations with temperature-dependent properties, a parameter study was conducted to investigate the influence of average material-property data. For this purpose, the coefficient of thermal expansion, α, the modulus of elasticity, E, and the yield curves were replaced in succession by average values in the elastoplastic FEM analysis. The reference temperature was 400°C. Figure 9(b) shows the influence of average values, taking the example of the longitudinal and equivalent strain curves at the base of the notch. During the heating phase, maximum differences of approximately 25 per cent result. The interaction of all three parameters as average values and a comparison with the completely non-linear calculation can be seen in Fig. 9(c).

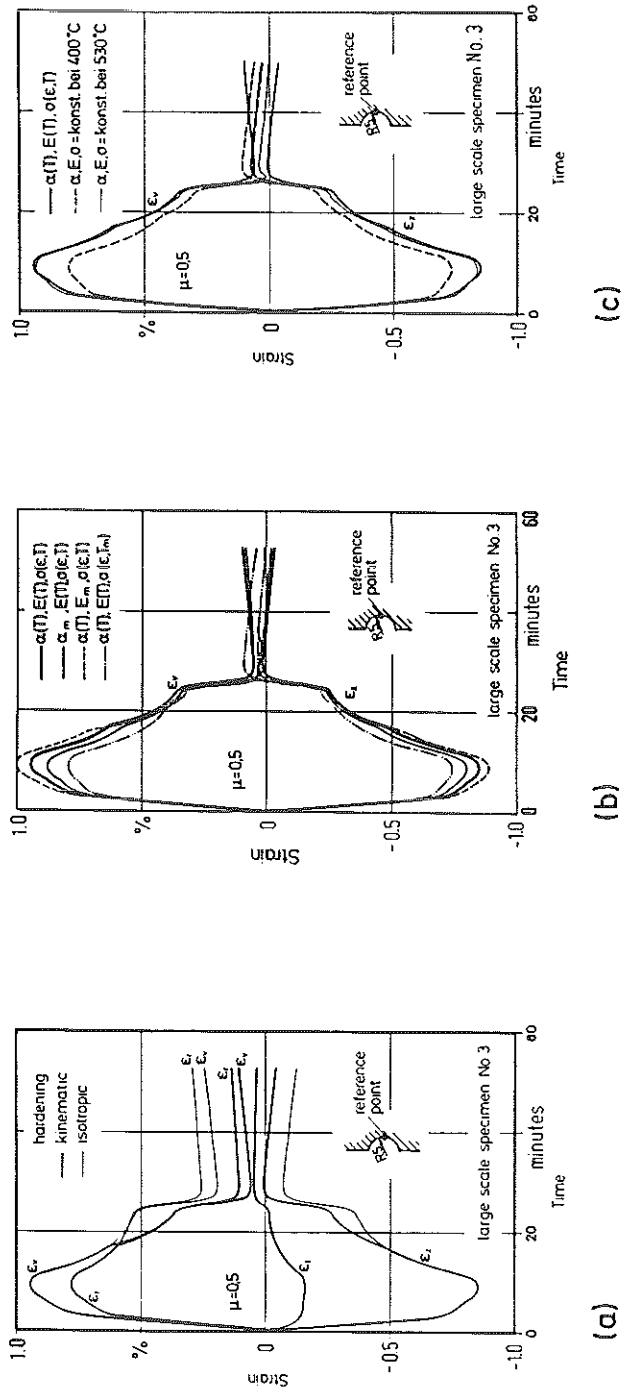

Fig 9 Strain vs time curves: (a) influence of the hardening rule; (b) influence of mean material data on calculated strains; (c) influence of mean stress–strain curves on the calculated strains

The use of average values causes the strains to be underestimated. Since the largest load at the base of the notch of the large scale specimen occurred during the highest temperature difference, a temperature of 530°C (which occurs in this specimen in the base of the notch) was used as a further reference temperature for a comparative calculation. This result is also shown in Fig. 9(c). In contrast to the calculation at 400°C, the strain curves are considerably closer to the curves in the more complex calculation. The reason for this is that the notable fall in the yield point occurs above 430°C and is reflected in an increase in the strains. The primary objective of the calculation with non-temperature-dependent materials data was to achieve a quantitative assessment of the yield point curve as a function of temperature, in order to derive an acceptable temperature for calculations. With a yield point which falls notably as the temperature increases, it can be assumed that the upper limit temperature represents the definitive calculation temperature. An incorrect choice of reference temperature for the calculation with constant materials data does not have as serious an effect on the results in the case of materials with a virtually temperature-independent yield point.

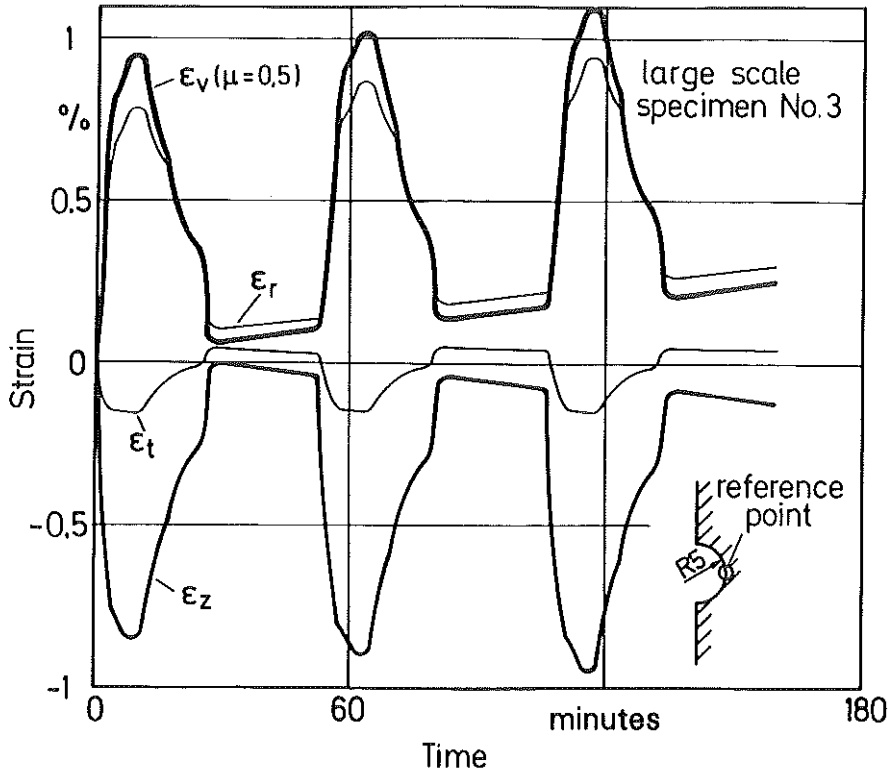

Fig 10 Strain components for three successive temperature cycles

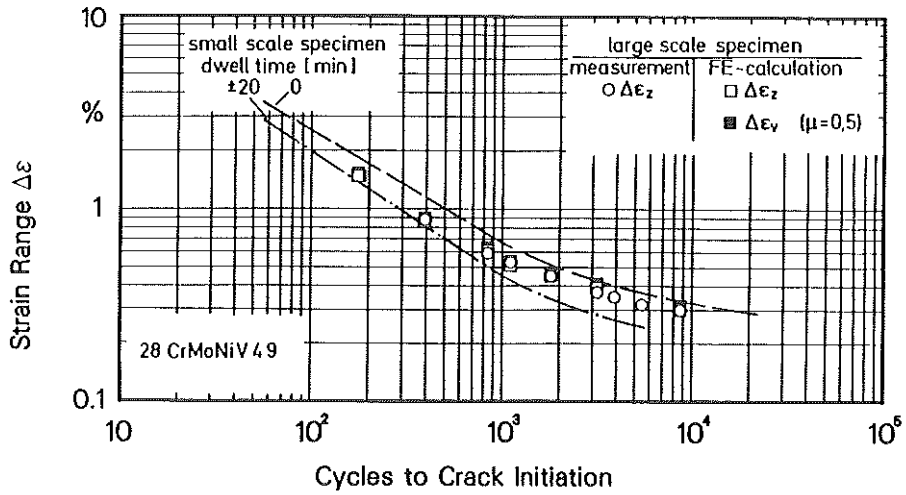

Fig 11 Comparison between the initiation curves for measured and calculated strains

The residual strains and stresses at the base of the notch after the first cycle mean that the following cycles are affected by the previous events in each case until saturation is reached. A calculation was carried with three successive cycles to provide more information concerning this behaviour. The strain components are shown in Fig. 10. In successive cycles, the axial stresses are increasingly shifted into the compression area; similarly the radial stresses are shifted into the tensile area. The circumferential strain, however, does not exhibit a displacement in its average value. It was not possible to detect a change in the strain amplitude.

In Fig. 11, the incipient crack behaviour is plotted with the theoretical amplitudes for an incipient crack depth of 1.0 mm; this is compared with axial isothermal laboratory experiments. Due to the good correlation between the measured and calculated axial strains, the individual points virtually coincide. The characteristic, based on the calculated equivalent strain with $\mu = 0.5$, deviates only slightly from the characteristic based on the axial strain.

Summary and conclusions

Thermally-loaded installations and components are subject to alternating strains which may be beyond the elastic limit at points of high strain concentration. To allow incipient crack characteristics to be examined at alternating temperatures, the turbine shaft was selected as a relatively simple axisymmetric component which was geometrically represented in miniaturized form by a test specimen. A specially-designed test stand made it possible to subject these large scale specimens to alternating temperatures. The incipient crack characteristics obtained by experiment were compared with the characteristics

obtained from axially loaded experiments at constant temperature. Fractographic inspection of fatigue cracks made it possible to utilize the fatigue striations obtained to determine the crack propagation rate. The quality of finite element calculations was investigated by an indirect comparison of the measured strains with the calculated strains. A subsequent parameter study, intended to illustrate the influence of average materials data on the calculated results, indicated that, if the temperature-dependent yield curves are retained, the physical characteristics of the large-scale specimens can be represented with sufficient accuracy, even with an average coefficient of thermal expansion and an average modulus of elasticity. Furthermore, a good approximation to the experimental results was obtained in the complex calculation in which the materials behaviour, including the yield curve, related to the upper limit temperature of the temperature cycle.

References

(1) STEGMEYER, R. (1987) The design and operation of a test facility for temperature cycling of large specimens, *Biaxial and Multiaxial Fatigue*, EGF 3 (Edited by BROWN, M. W. and MILLER, K. J.) 1989, Mechanical Engineering Publications, London, pp. 201–216. This volume.

(2) PARIS, P. C., ERDOGAN (1963) A critical analysis of crack propagation laws, *J. Basic Engng, Trans ASME*, **85**, 528–534.

(3) STEGMEYER, R. (1985) *Experimentelle und numerische Simulation des Bauteilverhaltens unter Wärmewechselbeanspruchung*, Techn.-wiss. Bericht, MPA Stuttgart, Heft 85-01 ISSN 0721-4529.

(4) BHONGBHIBHAT, S. (1979) *Untersuchungen über das Werkstoffverhalten im Gebiet der Zeitfestigkeit zur Erstellung von Berechnungsunterlagen für überwiegend thermisch beanspruchte Bauteile*, Dissertation, Universität Stuttgart.

(5) SZIMMAT, J. (1982) *SMART II.2, Instationäre Diffusion*, Benutzerhandbuch, ISD-Bericht Nr. 192, Stuttgart.

(6) *ASKA PART III 1 – Material Non-Linearities* (1979), (User's Reference Manual), ISD-Report No. UM 207, Stuttgart.